Absorption of Ultrashort Laser Pulses by Solid Targets Heated Rapidly to Temperatures 1–1000 eV

D. F. Price, R. M. More, R. S. Walling, G. Guethlein, R. L. Shepherd, R. E. Stewart, and W. E. White

Lawrence Livermore National Laboratory, Livermore, California 94550

(Received 4 April 1995)

We report measurements of laser absorption for high-contrast ultrashort pulses on a variety of solid targets over an intensity range of 10^{13} to 10^{18} W/cm^2. These data give an experimental determination of the target energy content and an indirect measure of dense plasma electrical conductivity. Our calculations accurately reproduce the behavior of aluminum targets, while the other materials show signs of additional absorption mechanisms. At high intensity all target materials reach a "universal plasma mirror" state and reflect about 90% of the incident light.

The development of high-power ultrashort pulse lasers has made possible a new type of laboratory investigation of the physical properties of matter heated rapidly to temperatures from 1 to 1000 eV, while retaining a density near that of the initial solid target [1,2]. Even before the development of subpicosecond pulse lasers it was shown that the reflectivity of a 30 ps probe pulse provides information on the ac electrical conductivity of the target plasma [3]. The first subpicosecond reflectivity experiments by Milchberg et al. [4], Fedosejevs et al. [5], Murnane, Kapteyn, and Falcone [6], and Teubner et al. [7] measured the reflectivity of aluminum and other materials at various conditions of laser intensity, pulse length, and prepulse. These experiments stimulated new theoretical calculations of dense plasma conductivity and some discussion about the key physical processes in these plasmas, as recently summarized by Ng et al. [8].

The scientific interest of these experiments centers on the possibility of using such short pulses that the uncertainty of plasma density is reduced at the time of peak laser intensity. Then one can directly measure properties of matter at exotic but known conditions.

The experiments reported here greatly extend the parameter range of this technique. The 120 fs (FWHM) laser pulses are significantly shorter or of higher contrast than previously used. The prepulse intensity contrast ratio is approximately 10^{-7} at 1 ps before the peak power, achieved by harmonic conversion of an already high contrast pulse described below. The intensity range of 10^{13}–10^{18} W/cm^2 enables us to unambiguously identify the interesting region of minimum mean free path at the transition from solid to plasma electronic structure. We report data for several materials (Fig. 1) and can begin to identify characteristic behavior of the different classes of materials.

At low intensities, 10^{13}–10^{14} W/cm^2, there is already evidence of some alteration of the cold-matter electronic structure; for example, quartz and other insulators have high absorption ($\sim$90%), very different from their room-temperature behavior. Above about 2×10^{15} W/cm^2, the reflectivity of each material has similar value and temperature dependence, consistent with a "universal plasma mirror" reflectivity of a sharp plasma-vacuum interface. The intermediate intensities are consistent with a minimum
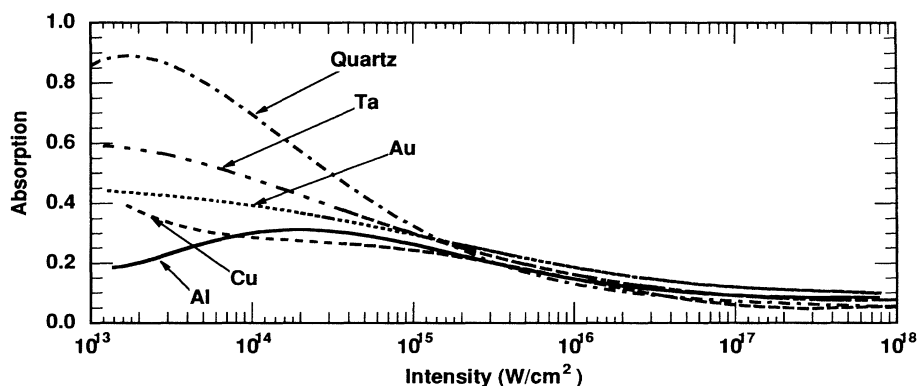

FIG. 1. Absorption fraction vs peak laser intensity for aluminum, copper, gold, tantalum, and quartz targets. In Figs. 1, 3, 4, and 5 laser intensity is the temporal and spatial peak value of the laser intensity.

     0031-9007/95/75(2)/252(4)$06.00   © 1995 The American Physical Society

electrical conductivity associated with an electron mean free path comparable to the interatomic spacing.

These experiments were performed at the LLNL Ultra-Short Pulse (USP) laser facility. The mode-locked cw-pumped Ti:sapphire oscillator produces near bandwidth-limited (9 nm FWHM at 800 nm) 4 nJ pulses in an 82 MHz pulse train. These pulses are stretched to 400 ps in a single diffraction grating pulse stretcher. One such chirped pulse is selected by polarization rotation and injected into a regenerative amplifier. After approximately 12 passes in the regenerative amplifier the pulse is extracted by a second firing of the Pockels cell. This light pulse also contains a series of prepulses separated by the cavity's round-trip time. Two additional Pockels cells are used to reduce the relative intensity of the prepulses to 10^{-9}. Two additional Ti:sapphire amplifier stages boost the uncompressed energy up to 200 mJ.

The amplified pulse is recompressed to approximately 120 fs FWHM in a parallel grating compressor with a throughput of 50%. The grating compressor is housed in a vacuum box to avoid self-phase-modulation and B-integral modulation of the beam. Transmittive optics are minimized to avoid B-integral modulation and self-phase-modulation of the beam and typically consist of the 0.15 cm doubling crystal, which operates at 41% efficiency, and two 0.1 cm beam splitters and a 5 μm thick nitrocellulose debris shield. The pulses are focused at normal incidence onto the target by an off-axis parabolic mirror ($f/4.8$) of 10.2 cm focal length.

We use several techniques to improve the pulse contrast. Leakage from the regenerative amplifier is measured and minimized as described above. Third- and fourth-order aberrations in the pulse stretcher introduce low-level temporal wings in the recompressed pulse. The wings are measured in a high dynamic range scanning autocorrelation of the 800 nm light. The 1ω pulse shape is calculated using the symmetric unfolding of the second order autocorrelation. Frequency doubling this light greatly improves the pulse contrast. The 400 nm temporal wave form shown in Fig. 2 is computed numerically with a nonstationary model of the second harmonic conversion process accounting for group velocity dispersion and pump pulse depletion [9]. This calculation gives a pulse that is slightly asymmetric and broadened by about 30 fs. The asymmetry and broadening arise due to the difference in group velocity dispersion between the fundamental and doubled light pulses propagating in a thick crystal, while the fundamental pulse experiences significant energy depletion. This calculated pulse shape is used in our theoretical simulations.

The target is enclosed in a light-integrating half cylinder of Lambertian scattering material. The scattered light is measured by a photodiode, which views a portion of the interior surface of the cylinder and is blocked from a direct view of the target. Incident, reflected and transmitted energies are monitored on each shot using pyroelectric
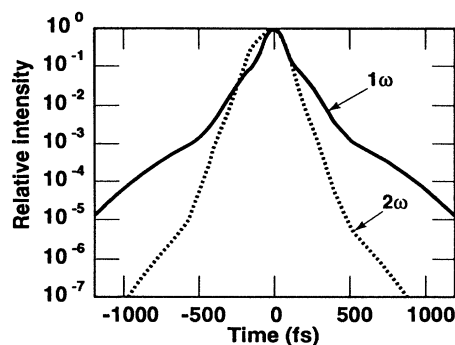

FIG. 2. Temporal pulse shape for 1ω and 2ω pulses. The 1ω pulse shape is inferred from a high dynamic range autocorrelation measurement and based on the assumption of a pulse symmetric in time. The 2ω pulse shape is calculated from the 1ω pulse shape and is slightly asymmetric because of group velocity dispersion and pump depletion [9].

energy meters. All energy meters are calibrated relative to the transmission meter, and transmission calibrations are made before and after each intensity scan (200 shots) so that a correction can be made for accumulated material on the debris shield (up to a 3% correction). The absorption is calculated as one minus the fractions of reflected, scattered, and transmitted light. The experimental measurements are time and space integrated.

Intensity is varied by moving the target on the converging side of best focus. This method of changing the intensity enables us to work with a large range of intensities. At best focus, we optically measure the focal spot diameter produced on target by an attenuated full power beam. The focal spot image is obtained by viewing a calibrated magnified image of the target through the final focusing objective. For the 400 nm pulse the smallest spot size is approximately 1.5 times the diffraction limit. Both the incoming and the focused light have an approximately Gaussian spatial profile. Spot diameters and Gaussian beam intensity distributions were also measured by knife-edge scans of the full-power beam over the entire range, from 10^{13} to 10^{18} W/cm^2, used in this work.

A typical data run consists of 100–200 measurements over an intensity range of 5 orders of magnitude. The target is scanned in order to ensure that clean material is exposed for each shot. The targets are electron-beam deposited films, 1 μm thick, on Kodak projector slide cover glass.

Figure 3 shows measured reflected and scattered light fractions and the inferred absorption for aluminum. As for most other targets, the scattered light is only about 2% of the incident light. The low scattering is evidence that the prepulse effects are small.

Figure 1 shows least-squares polynomial fits to the absorption data for Al, Cu, Au, Ta, and quartz. Experiments on several other ionic insulators give results similar to the quartz data: high absorption at low intensity, converging to the ideal plasma result at high intensity.
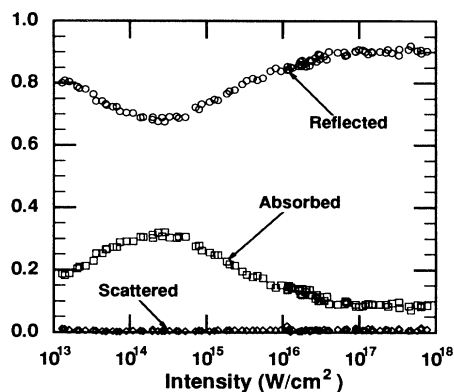
FIG. 3. Measured reflected and scattered energy fractions for an aluminum target vs peak laser intensity. Also shown are the corresponding absorption fractions.
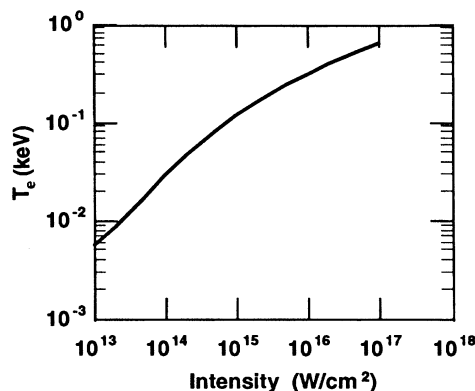

FIG. 4. The predicted spatial maximum electron temperature occurring at the temporal and spatial peak of the laser pulse plotted as a function of the peak laser intensity.

A detailed numerical simulation of the target inter-action has been performed for aluminum. The LASNEX one-dimensional Lagrangian hydrodynamics calculation includes the solution of the wave equation for the laser electromagnetic field using a theoretical model for the elec-trical conductivity of the target material, as described be-low. Heat flow is calculated as theoretical electron thermal conductivity without anomalous inhibition or modification. Numerical experiments show that a moderate heat-flux in-hibition would not greatly change our results. This is quite unlike the situation for longer pulse irradiation.

Our calculations take into account important spatial and temporal plasma variations, which are present in the experiments. Hydrodynamic expansion of the plasma is important except at the lowest intensities. A series of one-dimensional LASNEX simulations are integrated over the Gaussian focal-spot intensity distribution before comparison to the experiment. This final step gives a more realistic model of the experiment performed, in which radial transport is negligible, but where the radial intensity distribution significantly alters absorption.

The theoretical simulation uses the 2ω pulse shape shown in Fig. 2. The early wings of this pulse cause enough target heating to change the absorption by approxi-mately 10% of its value at the lower intensities. The cal-culations are performed using an additive two-temperature theoretical equation of state, described in Ref. [10]. This model gives better agreement with experiment than obtained by splitting an equilibrium (one-temperature) tabular equation of state. For most of our range, the ponderomotive pressure does not have a large effect, but it becomes important at the highest intensities or for longer pulses.

The peak temperature (maximum in space and time) in the theoretical calculations varies between 1 and 1000 eV as indicated in Fig. 4. The typical temperature in the heated material is significantly lower than this peak value.

Our LASNEX calculation uses inverse bremsstrahlung absorption or Ohmic heating based on a complex ac conductivity $\sigma(\omega)$ obtained by numerical evaluation of the Boltzmann-Drude formula,

$$\sigma(\omega) = \frac{n_e e^2}{m} \left\langle \frac{\tau(\epsilon)}{1 - i\omega\tau(\epsilon)} \right\rangle, \tag{1}$$

where $\tau(\epsilon)$ is an energy-dependent electron-ion collision time described by Lee and More [11]. In our calculation this collision time is evaluated with unequal electron and ion temperatures. The average in Eq. (1) is taken over the electron energy distribution function and includes effects of Fermi statistics at low temperatures.

The results of these calculations agree with the ex-periment up to intensities of 10^{17} W/cm^2 for aluminum (Fig. 5).

The aluminum target interaction in this model is entirely due to Ohmic heating of the free electrons by the laser electric field. Our calculation of this mechanism does not account for all of the absorption observed for other target materials.

For Cu, Au, and Ta the experiment shows additional low intensity absorption beyond that predicted by the Ohmic heating process. Guided by the known proper-ties of the cold materials, it is reasonable to attribute this extra absorption to intra-atomic absorption (e.g., $3d$-$4p$ transitions in Cu), which decreases with tempera-ture because the relevant atomic levels move to larger energy separation. The details will be presented else-where [12]. For the ionic insulators [13], the high ab-sorption (90%) is evidently due to a thick absorbing region (>1000 Å) containing an underdense electron gas produced at the low intensities of 10^{13} W/cm^2. At higher intensities the electron density rises and the targets switch to metallic-plasma behavior with a skin depth of 100 Å and a substantial reflectivity. A de-tailed model for these materials will be described else-where [14].
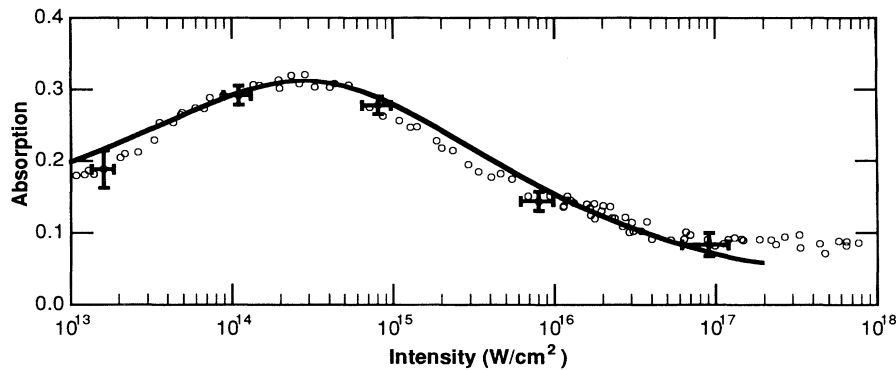
FIG. 5. Measured and calculated absorption fractions for an aluminum target vs peak laser intensity. The calculation assumes a Gaussian laser spatial profile. Error bars shown indicate systematic uncertainty in intensity and random error in absorption. The absolute absorption scale is believed to be known to ±0.035.

An experiment on Al_2O_3, not shown in Fig. 1, gives high absorption similar to the other ionic insulators. In this region of high absorption, the deep penetration of the electromagnetic field, required to avoid generating reflected light, implies that a thin oxide layer would not have significantly affected the aluminum metal data shown in Figs. 3 and 5.

The results presented in this paper clearly show the possibilities for ultrashort pulse laser absorption experiments, but leave many questions for future work. For a simple metal like aluminum, we find excellent agreement with numerical simulations using inverse bremsstrahlung absorption. In insulators and in complex metals, other absorption processes are clearly present. Future measurements are needed to completely understand the absorption mechanisms, material properties, and energy transport in these high density plasmas.

[1] D. Strickland and G. Mourou, Opt. Commun. **56**, 219 (1985).
[2] R. M. More *et al.*, J. Phys. (Paris), Colloq. **61**, C7-43 (1988).
[3] A. Ng *et al.*, Phys. Rev. Lett. **57**, 1595 (1986).
[4] H. M. Milchberg, R. R. Freeman, S. C. Davey, and R. M. More, Phys. Rev. Lett. **61**, 2364 (1988).
[5] R. Fedosejevs *et al.*, Phys. Rev. Lett. **64**, 1250 (1990).
[6] M. M. Murname, H. C. Kapteyn, and R. W. Falcone, Phys. Fluids B **3**, 2409 (1991).
[7] U. Teubner *et al.*, Phys. Rev. Lett. **70**, 794 (1993).
[8] A. Ng *et al.*, Phys. Rev. Lett. **72**, 3351 (1994).
[9] K. Goldberg, senior thesis, University of California, Berkeley, 1992; R. Falcone (private communication).
[10] R. M. More, K. H. Warren, D. A. Young, and G. B. Zimmerman, Phys. Fluids **31**, 3059 (1988).
[11] Y. T. Lee and R. M. More, Phys. Fluids **27**, 1273 (1984); R. M. More, in *Handbook of Plasma Physics*, edited by M. Rosenbluth, R. Sagdeev, A. Rubenchik, and S. Witkowski (Elsevier, Amsterdam, 1991), Vol. 3.
[12] Z. Zinamon *et al.* (private communication).
[13] B.-T. Vu, O. L. Landen, and A. Szoke, Phys. Plasmas **2**, 476 (1995).
[14] Z. Zinamon *et al.* (private communication).